

Supporting information

Contrasting the EXAFS obtained under air and H₂ environments to reveal details of the surface structure of Pt-Sn nanoparticles

Haoliang Huang¹, Abu Bakr Ahmed Amine Nassr^{1,2}, Verónica Celorrio³, Diego Gianolio³,
Christopher Hardacre⁴, Dan J. L. Brett⁵, Andrea E. Russell*¹

¹ School of Chemistry, University of Southampton, Highfield, Southampton, SO17 1BJ, UK

² Fraunhofer Institute for Microstructure of Materials and System, Walter-Hülse-Straße 1, 06120 Halle
(Saale), Germany

³ Diamond Light Source Ltd. Diamond House. Harwell Campus. Didcot, OX11 0DE, UK

⁴ School of Natural Sciences, The University of Manchester, The Mill, Manchester, M13 9PL, UK

⁵ Department of Chemical Engineering, University College London (UCL), London, WC1E 7JE, UK

Corresponding author:

* E-mail: a.e.russell@soton.ac.uk (AER)

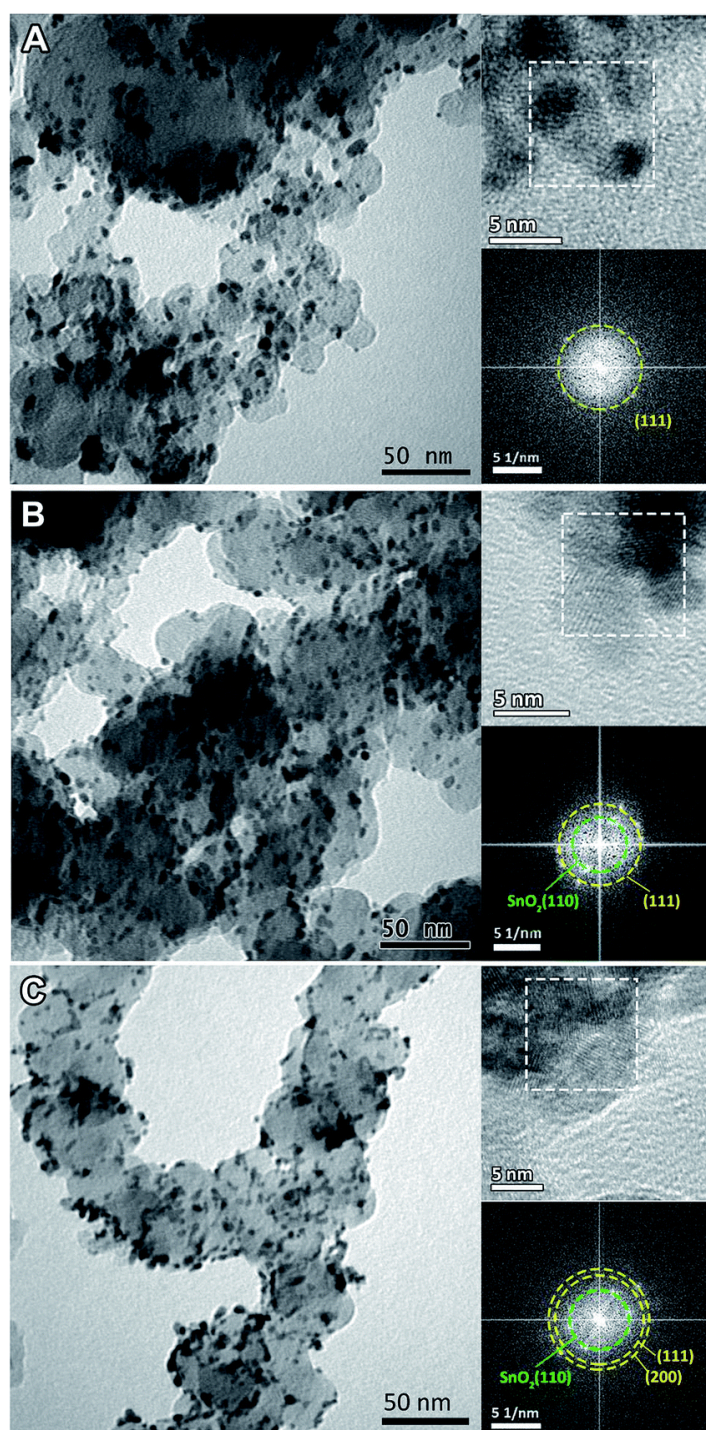


Figure S1 TEM images of the Pt-Sn bimetallic nanoparticles with different extents of alloying, (A) well-alloyed nanoparticles, (B) partly alloyed nanoparticles and (C) dealloyed nanoparticles, along with (the upper insets) the corresponding HRTEM images and (the bottom insets) the fast-Fourier transform patterns on the selected area. The average particle sizes were ~ 6 nm for the well-alloyed nanoparticles, ~ 5 nm for the partly alloyed nanoparticles and ~ 3 nm for the dealloyed nanoparticles. Reproduced from our previous work¹, which is licensed under a [Creative Commons Attribution 3.0 Unported Licence \(CC BY 3.0\)](https://creativecommons.org/licenses/by/3.0/)

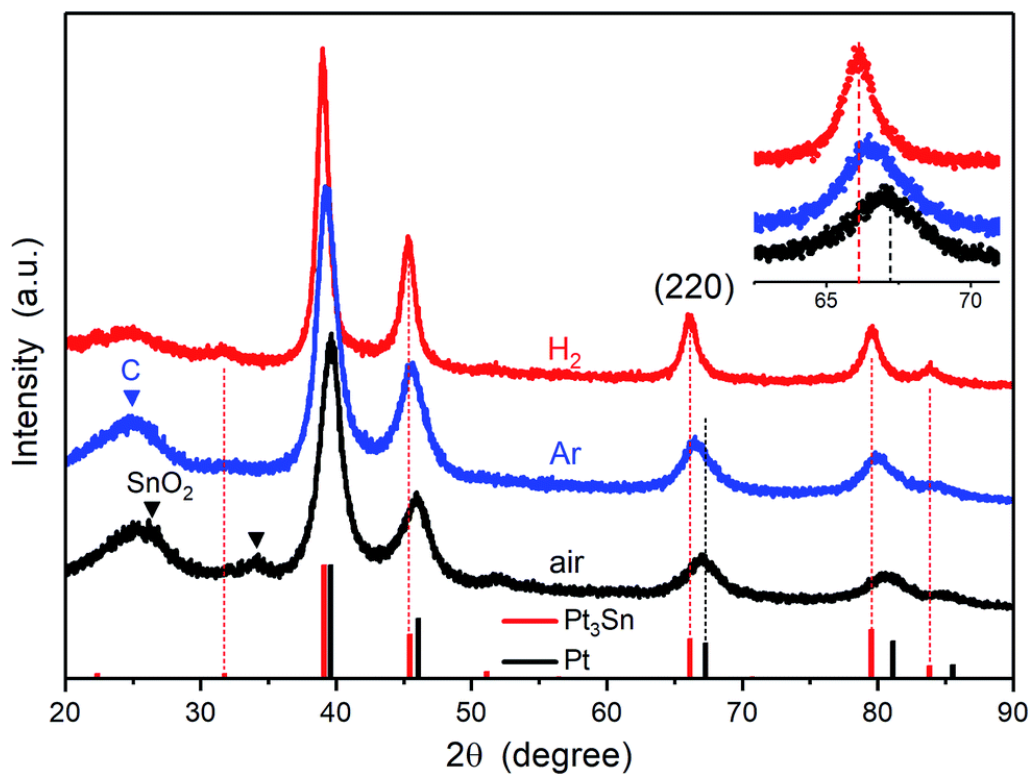


Figure S2 XRD patterns of the Pt-Sn bimetallic nanoparticles with different extents of alloying, (red, H₂) the well-alloyed nanoparticles, (blue, Ar) the partly alloyed nanoparticles, and (black, air) the dealloyed nanoparticles. The standard patterns of Pt₃Sn (35-1360) and Pt (04-0802) were obtained from the JCPDS database, and the inset shows the magnified region of the (220) peak. Reproduced from our previous work¹, which is licensed under a [Creative Commons Attribution 3.0 Unported Licence \(CC BY 3.0\)](https://creativecommons.org/licenses/by/3.0/).

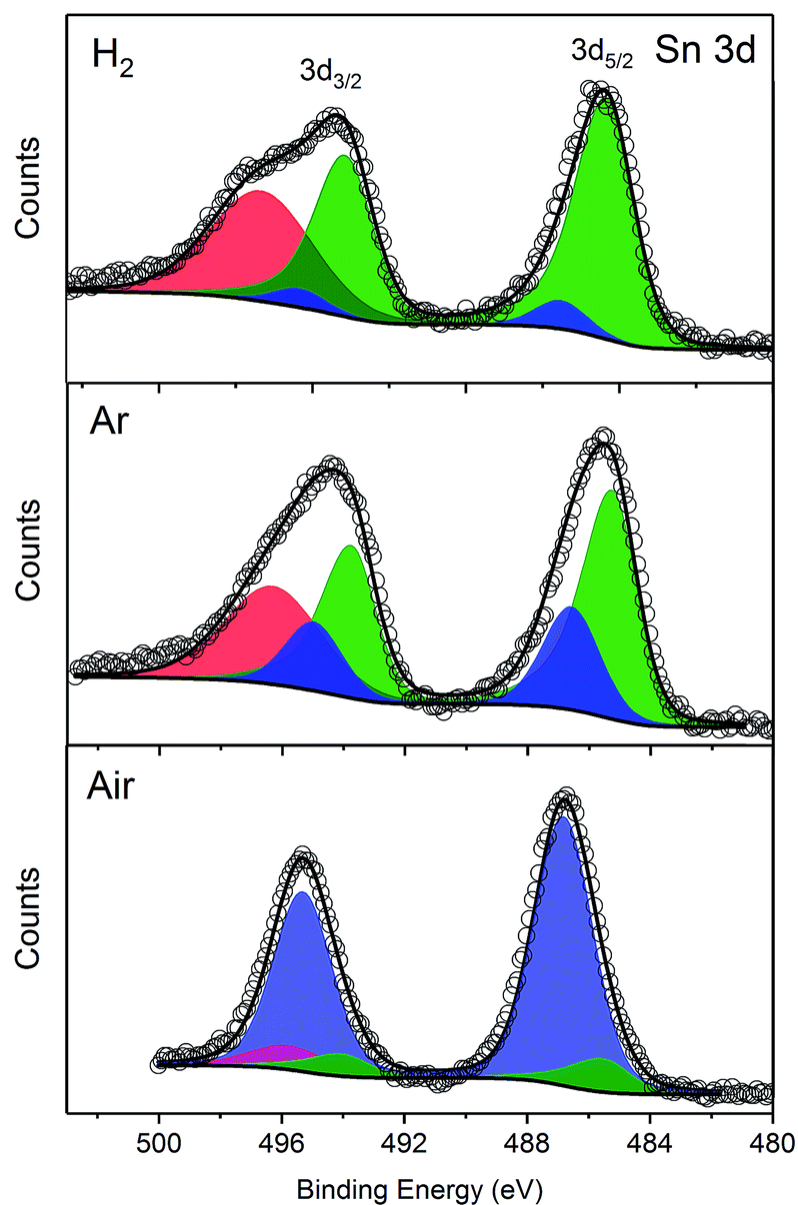


Figure S3 Sn 3d XPS spectra of the Pt-Sn bimetallic nanoparticles with different extents of alloying, (H₂) the well-alloyed nanoparticles, (Ar) the partly alloyed nanoparticles, and (air) the dealloyed nanoparticles. Peak deconvolution shown corresponding to Sn⁰ (green), Sn^{IV} (blue), and the loss feature of metallic Sn (red). Reproduced from our previous work¹, which is licensed under a [Creative Commons Attribution 3.0 Unported Licence \(CC BY 3.0\)](https://creativecommons.org/licenses/by/3.0/).

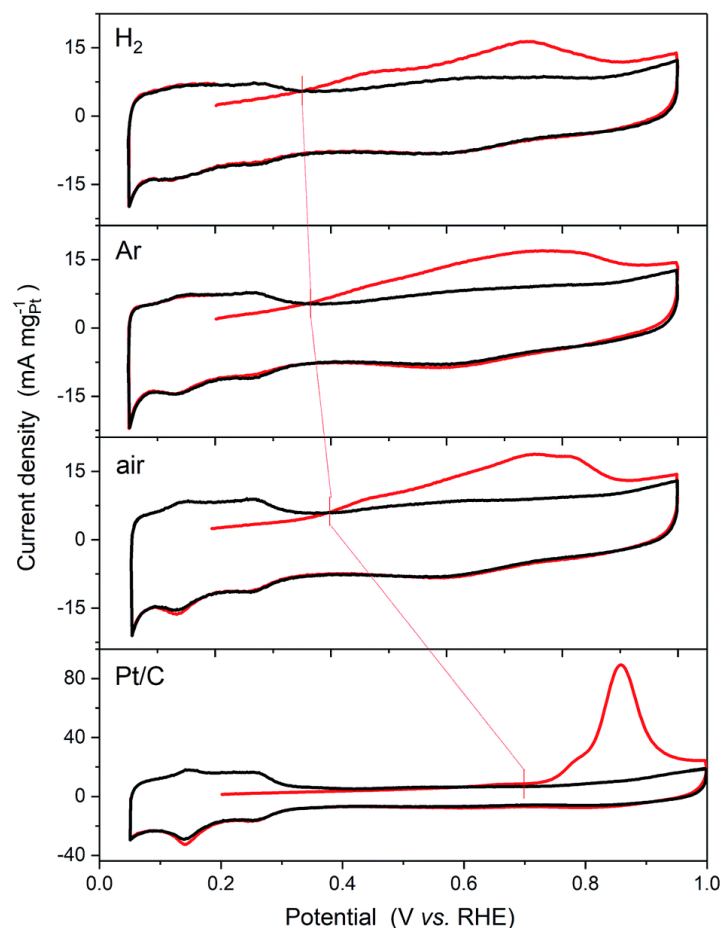


Figure S4 CO stripping voltammograms of the Pt-Sn bimetallic nanoparticles with different extents of alloying, (H₂) the well-alloyed nanoparticles, (Ar) the partly alloyed nanoparticles, and (air) the dealloyed nanoparticles, and a commercial Pt/C (20 wt%, JM). A saturated layer of CO is adsorbed at 0.2 V vs. RHE, and the measurements were carried out in 1 M H₂SO₄ with a scan rate of 20 mV s⁻¹.

The first cycles, starting at 0.2 V, are shown in red and the third cycles are shown in black. Reproduced from our previous work¹, which is licensed under a [Creative Commons Attribution 3.0 Unported Licence \(CC BY 3.0\)](https://creativecommons.org/licenses/by/3.0/).

Table S1 Comparison of electrochemical active surface area (ECSA) calculated from the charge related to CO stripping and Pt-H desorption. While these two values are equal within the error of the measurement, significant deviations are observed for the Pt-Sn samples and the ratio of these values increase with increasing the extent of alloying, which can be attributed to the dilution of surface Pt sites (active for H adsorption and CO adsorption) by the inactive Sn atom due to alloying. Reproduced from our previous work¹, which is licensed under a [Creative Commons Attribution 3.0 Unported Licence \(CC BY 3.0\)](#).

Samples	ECSA_{CO} (m² g_{Pt}⁻¹)	ECSA_H (m² g_{Pt}⁻¹)	ECSA_{CO}/ECSA_H
Alloyed Pt-Sn	25.1	7.4	3.4
Partly alloyed Pt-Sn	26.1	8.4	3.1
Dealloyed Pt-Sn	29.5	12.8	2.3
Pt/C	67.2	60.7	1.1

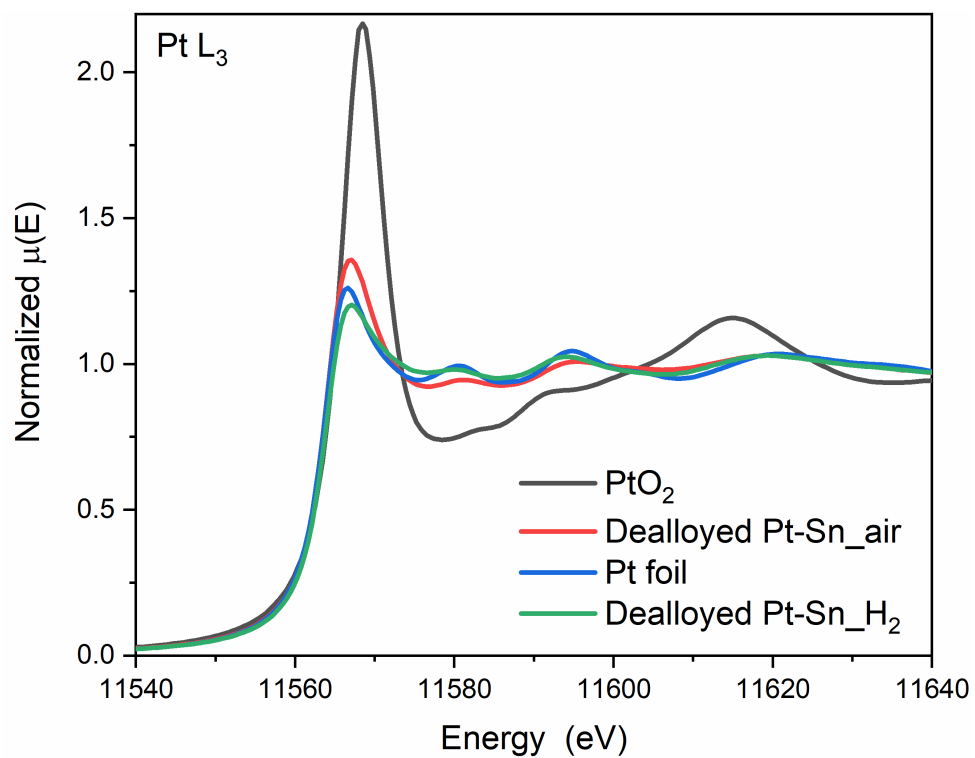


Figure S5 XANES of the dealloyed Pt-Sn sample at Pt L₃-edge, along with Pt foil and PtO₂ references.

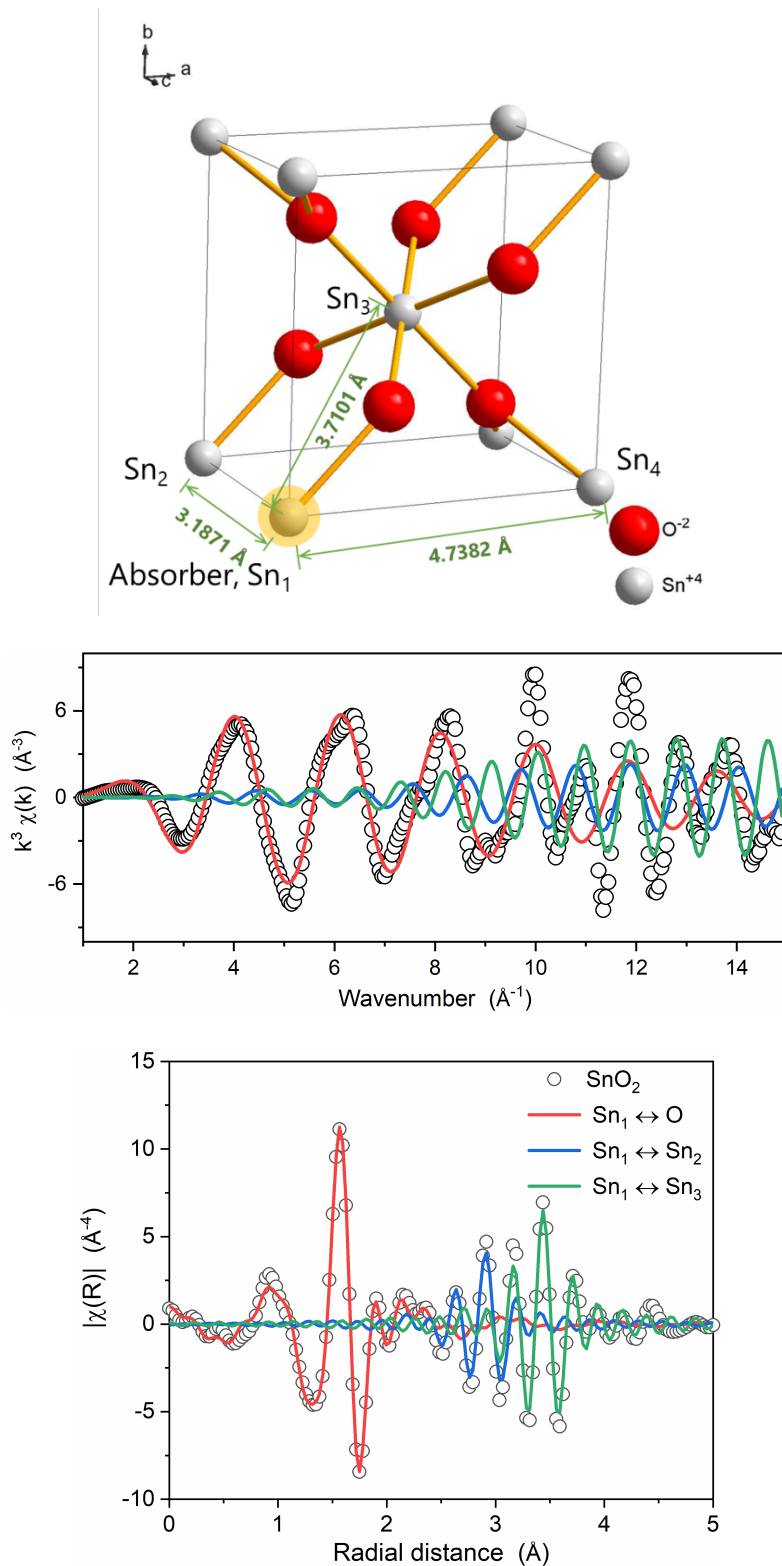


Figure S6 (top) A unit cell of rutile SnO₂ (ICSD 647469) and the EXAFS spectrum (middle) in k space and (bottom) in R space (real part), showing the contribution of different scattering paths to the EXAFS spectrum.

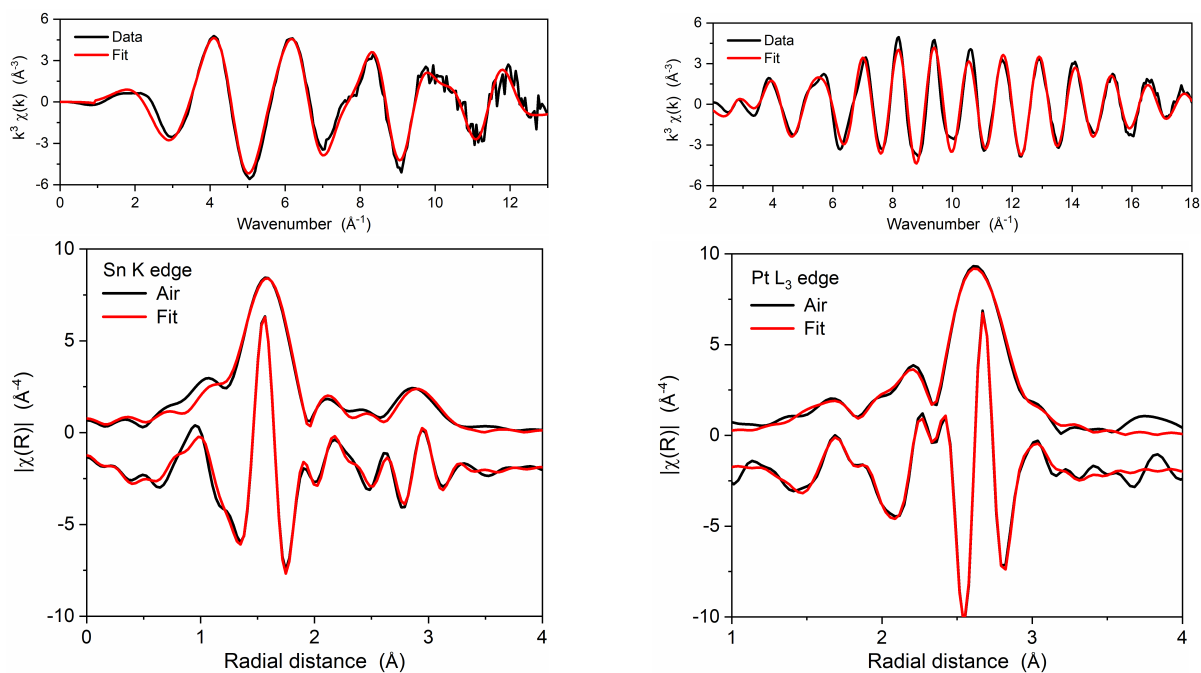


Figure S7 A double-dataset fit for the dealloyed Pt-Sn data measured in air, combining the EXAFS spectra collected at (left column) Sn K edge and (right column) Pt L₃-edge. The fit is shown in both (top) k^3 -weighted EXAFS spectra and (bottom) their Fourier transforms plotted as the magnitude and the real part (offset toward lower magnitude for clarity), and the Fourier transformation was carried out in k -ranges of 3.6–12.4 Å⁻¹ for the Sn K-edge and of 3.5–18.0 Å⁻¹ for the Pt L₃-edge. The fit was performed in R ranges of 1.2–3.2 Å for the Sn K-edge and of 1.2–3.0 Å for the Pt L₃-edge, yielding an R-factor of 0.27% and the obtained structural parameters listed in Table 1.

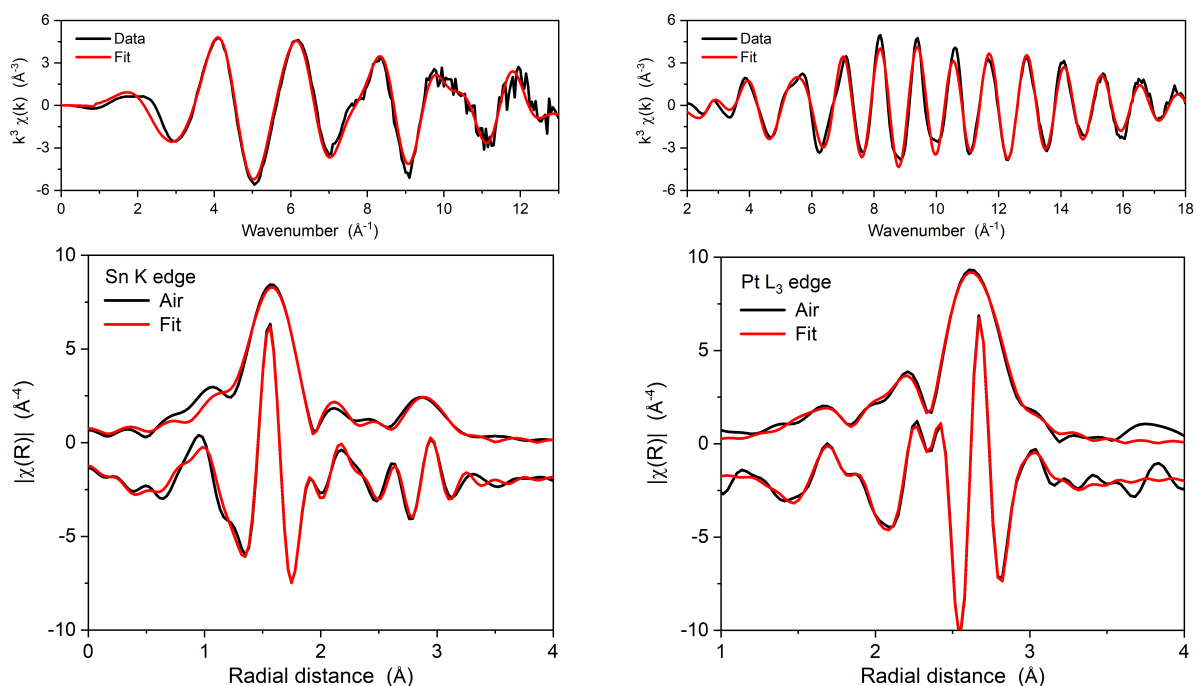


Figure S8 Same as Figure S7 but without a constraint in $N(\text{Sn-Pt})$. The fit yields an R-factor of 0.24% and the obtained structural parameters listed in Table S2.

Table S2 Structural parameters obtained from individual double-dataset fits of the dealloyed Pt-Sn data collected in air, without a constraint in $N(\text{Sn-Pt})$. The fits use 18 variables out of ~ 27 independent points for the data collected in air.

Samples	Scattering path	N	R (Å)	σ^2 ($\times 10^3$ Å ²)	ΔE_0 (eV)	R -factor (%)
Dealloyed Pt-Sn (air)	Pt – O	0.8(1)	1.996(6)	5(2)		0.24
	Pt – Pt	7.6(3)	2.757(2)	7.6(2)	7.3(4)	
	Pt – Sn	0.9(7)	2.83(2)*	19(11)*		
	Sn – O	5.0(7)	2.04(1)	5(2)		
	Sn – Pt	4(5)**	2.83(2)*	19(11)*	3(2)	
	Sn – Sn	1(1)	3.23(3)	6(7)		

* Pt – Sn and Sn – Pt scattering paths are set to have the same value in R and σ^2 .

** not constrained.

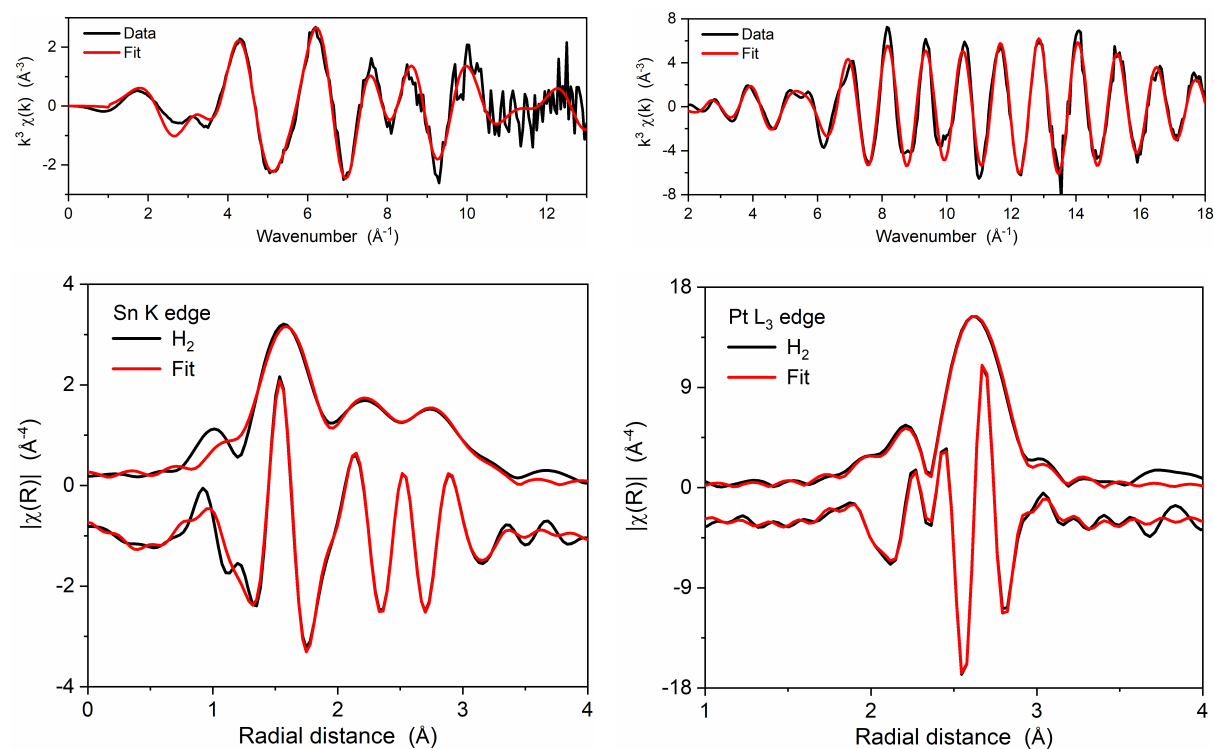


Figure S9 Same as Figure S7 but for the data measured in H₂ and with an R-factor of 0.22%.

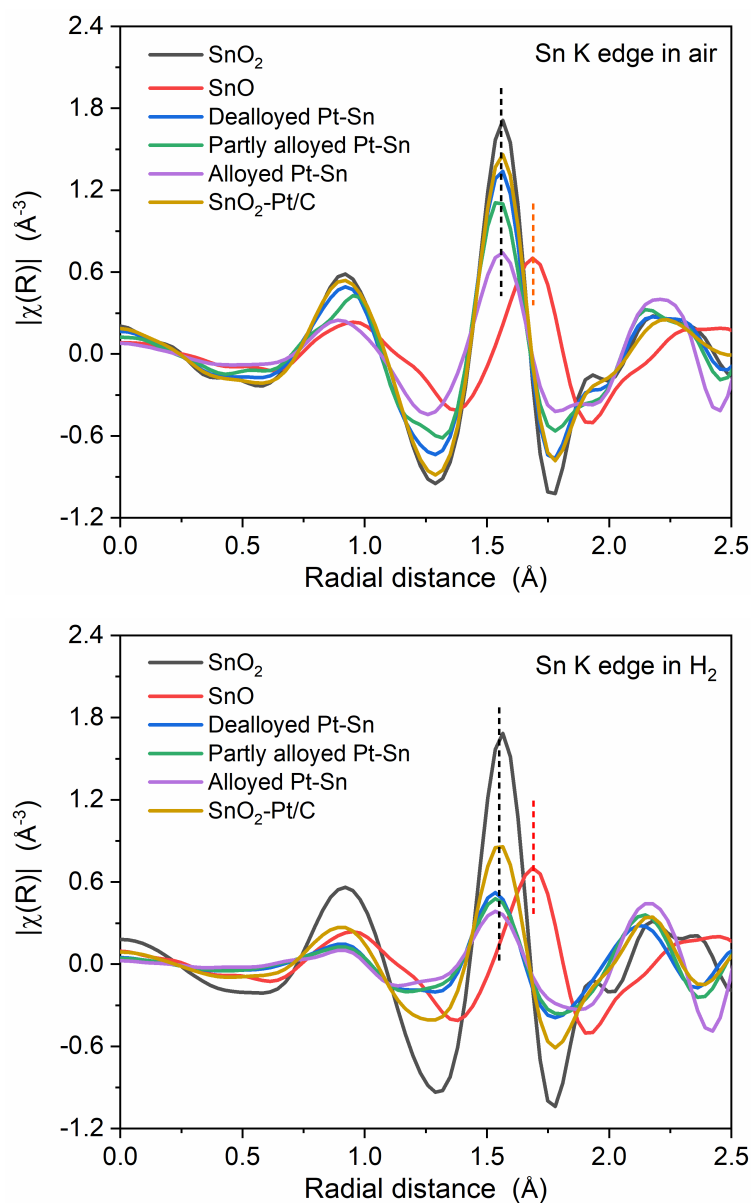


Figure S10 Fourier-transforms (the real part) of EXAFS spectra of the SnO₂ samples measured (top) in air and (bottom) in H₂, along with SnO₂ and SnO references (measured in air). The Fourier transformation was carried out in a k -range of 3.4–13.2 \AA^{-1} . These two figures compare the Sn–O oscillation of Pt–Sn samples presented herein, showing the position of Sn–O aligns with that of SnO₂ regardless of samples and measurement atmospheres, and is significantly smaller than that of SnO. This suggests that Sn^{II}-O are unlikely to present in our samples.

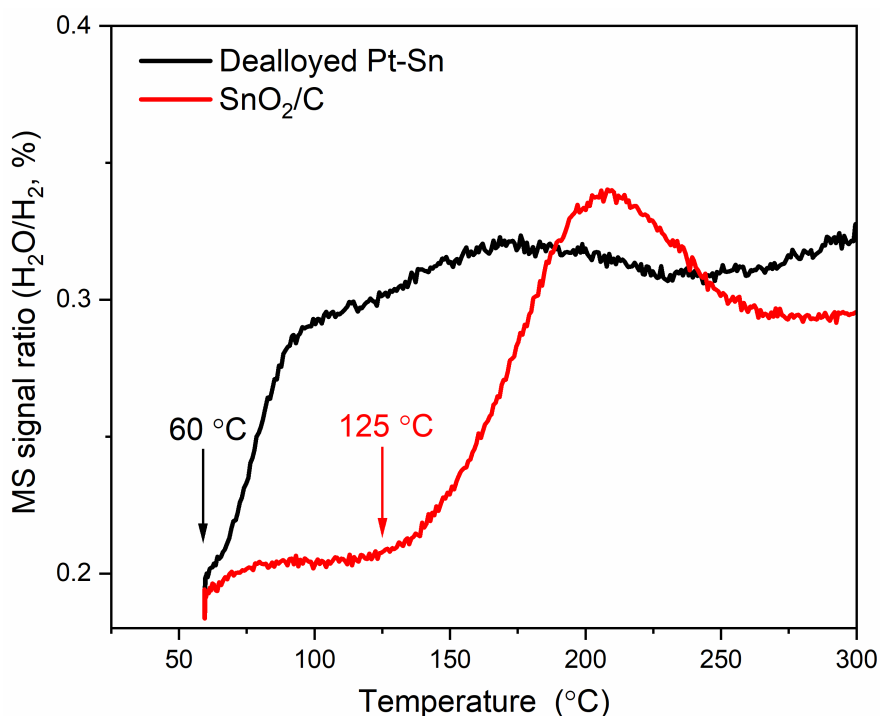


Figure S11 H_2 temperature-programmed reduction (TPR) of the dealloyed Pt-Sn and a SnO_2/C reference sample in a flowing H_2/He mixed gas ($4 \text{ ml min}^{-1} \text{ H}_2$ and $30 \text{ ml min}^{-1} \text{ He}$). The H_2 -TPR profile shows that the onset temperature of tin oxide reduction on SnO_2/C is much higher than that on the dealloyed Pt-Sn, suggesting that the involvement of Pt facilitate the reduction of SnO_2 , and implying the reduction of H_2 is likely to be unfavourable at low temperature if Pt is not involved. The H_2 -TPR was performed on CATLAB (RCaH), a microreactor system integrating with a mass spectrometer and a precise gas flow control. The samples were dried at $120 \text{ }^\circ\text{C}$ in $30 \text{ ml min}^{-1} \text{ He}$ for 20 min and allowed to cool down naturally to $60 \text{ }^\circ\text{C}$. The gas was then switched the mixed H_2/He gas and the temperature was stabilized for 10 min, to reduce Pt surface oxide before temperature program started. After that, the temperature was increased to $400 \text{ }^\circ\text{C}$ with a ramping rate of $5 \text{ }^\circ\text{C min}^{-1}$. This mass spectrometer signals of H_2 and H_2O were started to collect after the temperature stabilization started.

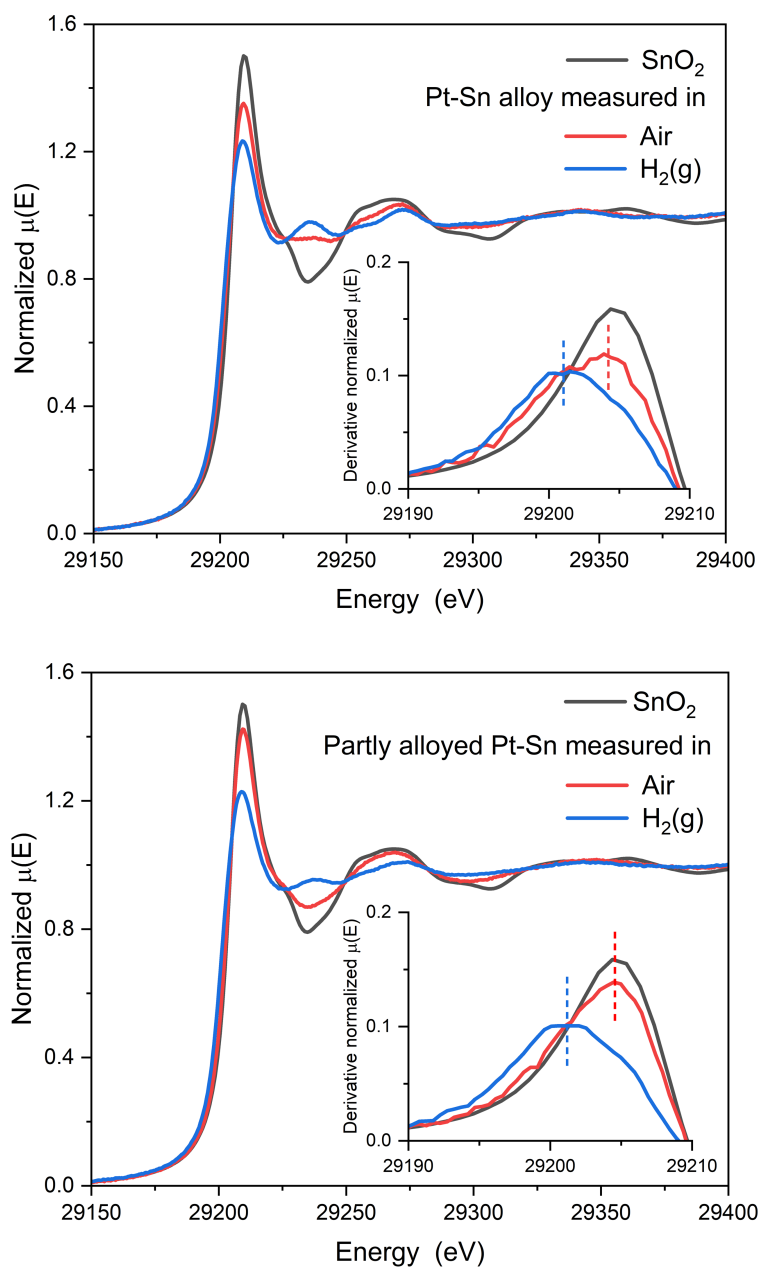


Figure S12 XANES spectra of (top) Pt-Sn alloy and (bottom) partly alloyed Pt-Sn samples, measured in air and in H₂, along with (inset) their 1st derivative at the rising edge. For the data measured in air, the extent of alloying is indicated by the decrease of the whiteline intensity and the lower-energy shoulder of the 1st derivative. The extents of decrease in whiteline intensity and of negative shift in edge position are less than those of the dealloyed one, indicating that less Sn^{IV} is reduced.

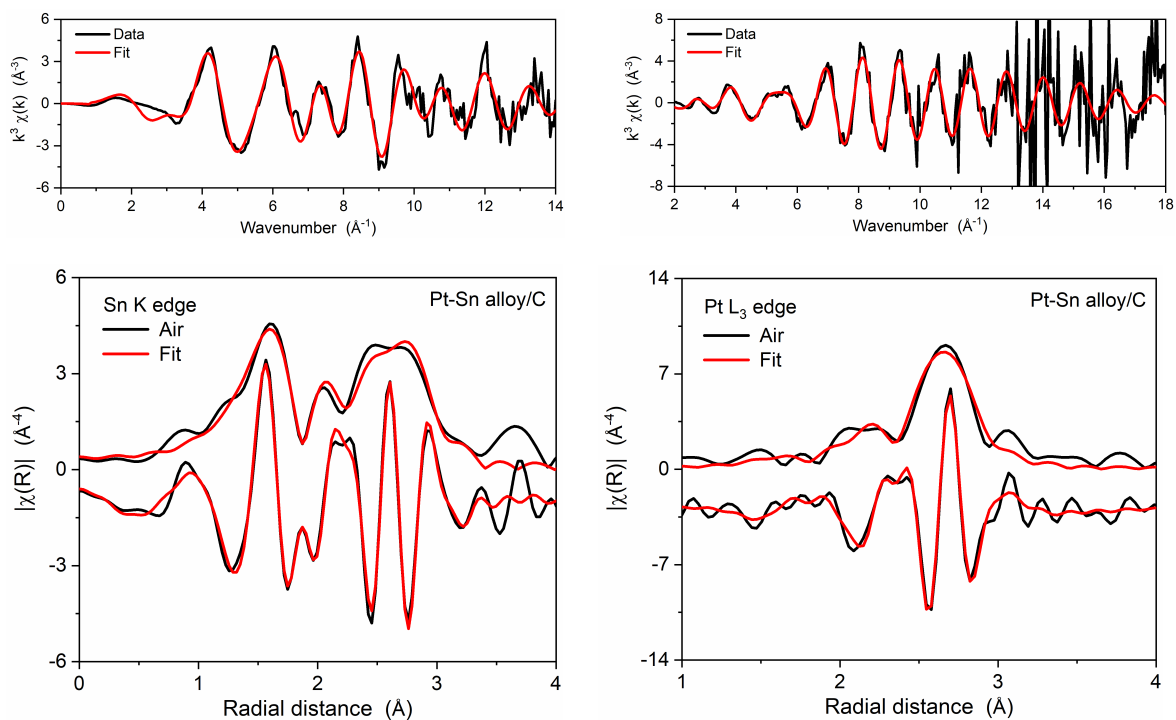


Figure S13 Same as Figure S7 but for Pt-Sn alloy data measured in air, and the Fourier transformation was carried out in a k -range of $3.6\text{--}13.7 \text{ \AA}^{-1}$ for the Sn K-edge and $3.5\text{--}17.3 \text{ \AA}^{-1}$ for the Pt L_3 -edge. The fit yields an R-factor of 1.13% and the obtained structural parameters listed in Table S3.

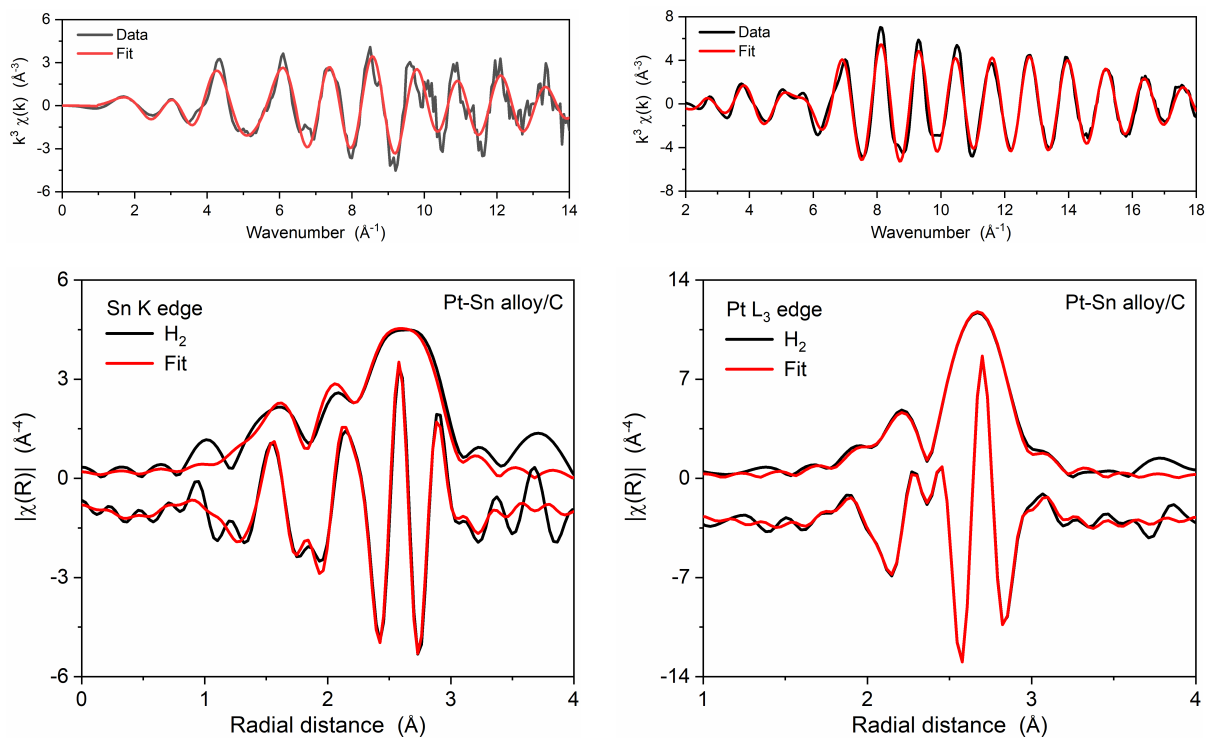


Figure S14 Same as Figure S13 but for Pt-Sn alloy data measured in H_2 . The fit yields an R-factor of 0.56%.

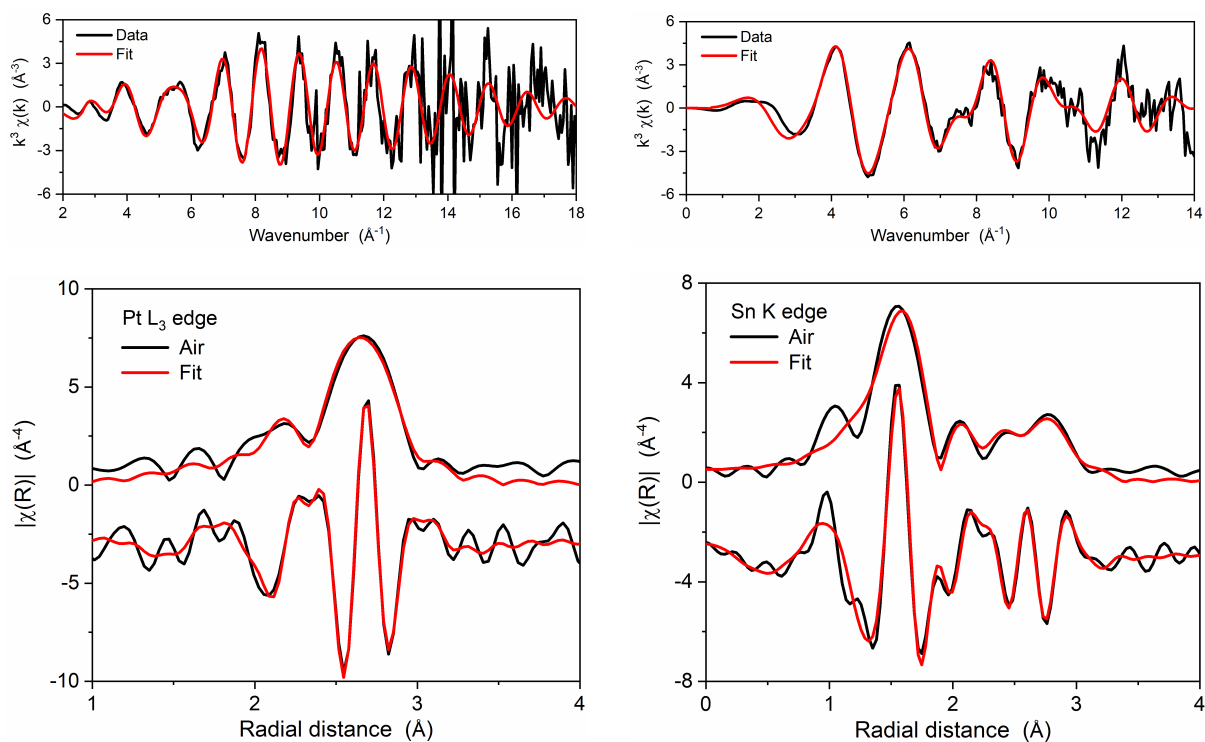


Figure S15 Same as Figure S7 but for partly alloyed Pt-Sn data measured in air, and the Fourier transformation was carried out in a k -range of $3.6\text{--}13.7 \text{\AA}^{-1}$ for the Sn K-edge and $3.5\text{--}16.2 \text{\AA}^{-1}$ for the Pt L_3 -edge. The fit yields an R-factor of 1.25% and the obtained structural parameters listed in Table S3.

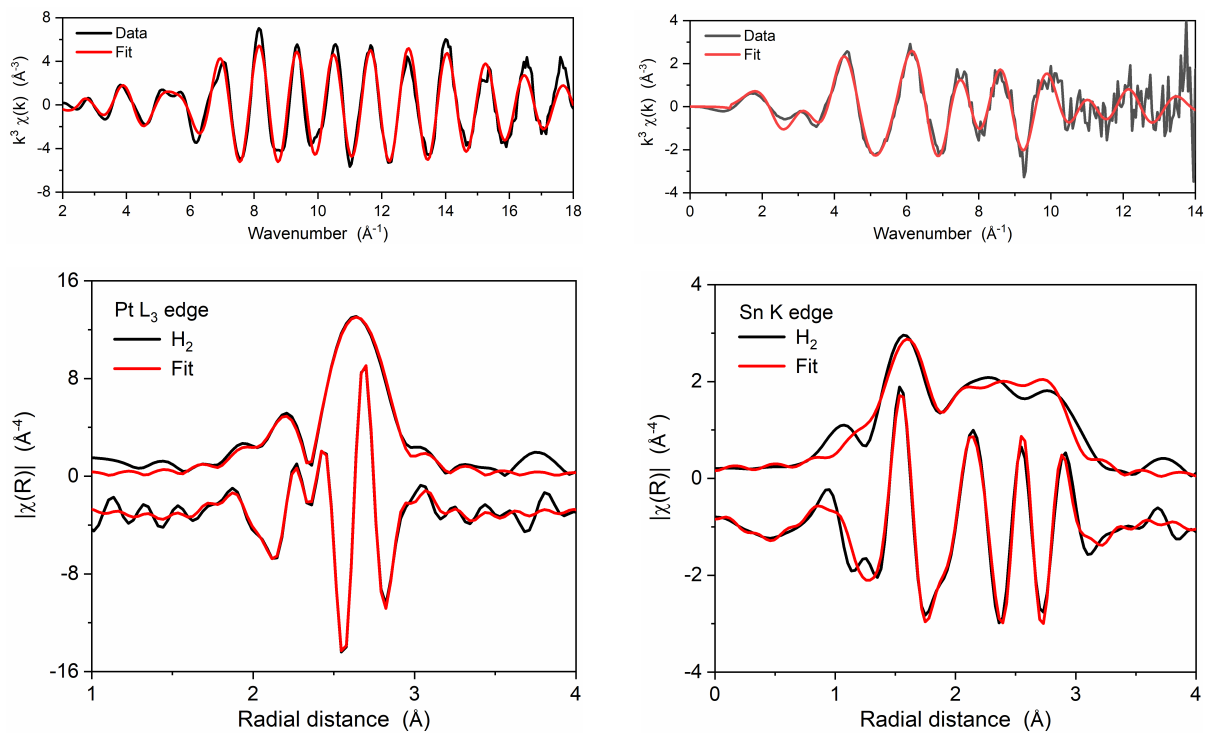


Figure S16 Same as Figure S7 but for partly alloyed Pt-Sn data measured in H_2 , and the Fourier transformation was carried out in a k -range of $3.6\text{--}13.2 \text{\AA}^{-1}$ for the Sn K-edge and $3.5\text{--}17.3 \text{\AA}^{-1}$ for the

Pt L₃-edge. The fit yields an R-factor of 1.25% and the obtained structural parameters listed in Table S3.

Table S3 Structural parameters obtained from double-dataset fits for alloyed Pt-Sn and partly alloyed Pt-Sn samples measured in air and in H₂. For the fits of alloyed Pt-Sn, 18 variables were used out of ~28 independent points for the data collected in air and 12 out of ~28 for the data collected in H₂. For the fits of partly alloyed Pt-Sn, 18 variables were used out of ~27 independent points for the data collected in air and 12 out of ~24 for the data collected in H₂.

Samples	Scattering path	<i>N</i>	<i>R</i> (Å)	σ^2 ($\times 10^3$ Å ²)	ΔE_0 (eV)	<i>R</i> -factor (%)
Alloyed Pt-Sn (air)	Pt – O	0.3(6)	1.99(8)	5(21)		1.13
	Pt – Pt	7(1)	2.77(1)	8(1)	5(2)	
	Pt – Sn	1.3(7)	2.808(4)*	9.7(7)*		
	Sn – O	2.9(2)	2.042(5)	6.3(8)		
	Sn – Pt	6.1(6)	2.808(4)*	9.7(7)*	2.5(6)	
	Sn – Sn	1.6(6)	3.28(2)	13(4)		
Alloyed Pt-Sn (H ₂)	Pt – Pt	7.8(2)	2.778(2)	6.7(2)	4.8(3)	0.56
	Pt – Sn	2.0(2)	2.790(5)*	10(1)*		
	Sn – O	1.0(6)	2.03(3)	5(7)	4(1)	
	Sn – Pt	8(1)	2.790(5)*	10(1)*		
Partly alloyed Pt-Sn (air)	Pt – O	1(2)	2.0(1)	14(40)		1.25
	Pt – Pt	7(2)	2.77(2)	8(1)	7(3)	
	Pt – Sn	0.8(8)	2.802(8)*	10(2)*		
	Sn – O	4.4(3)	2.037(6)	5.6(7)		
	Sn – Pt	3.4(9)	2.802(8)*	10(2)*	1.7(9)	
	Sn – Sn	3(2)	3.25(3)	20(10)		
Partly alloyed Pt-Sn (H ₂)	Pt – Pt	8.2(2)	2.764(2)	6.5(1)	5.0(3)	0.63
	Pt – Sn	1.3(2)	2.775(8)*	14(2)*		
	Sn – O	1.7(5)	2.04(2)	6(3)	5(1)	
	Sn – Pt	7(1)	2.775(8)*	14(2)*		

*The interatomic scattering paths are set to be equal in *R* and σ^2 for samples measured in the same atmosphere, that is, $R(\text{Pt-Sn}) = R(\text{Sn-Pt})$ and $\sigma^2(\text{Pt-Sn}) = \sigma^2(\text{Sn-Pt})$.

Table S4 The fitting model and guessed parameters, used in the 4-dataset fit of the dealloyed Pt-Sn sample.

Samples	Scattering path	N	ΔE_0	ΔR	σ^2
Pt L₃ in air	Pt – O	amppto	enotpt	delrpto	sspto
	Pt – Pt	amppt*		delrpt*	sspt*
	Pt – Sn	ampptsn*		delrptsn*.*.*.*	ssptsn*.*.*.*
Sn K in air	Sn – O	6×ampsno	enotsn	delrsno**	sssno**
	Sn – Pt	12×(1-ampsno)*		delrptsn*.*.*.*	ssptsn*.*.*.*
	Sn – Sn (2 nd shell)	ampsnsn		delrsnsn**	sssnsn**
Pt L₃ in H₂	Pt – Pt (core)	amppt*	enotpth2	delrpt*	sspt*
	Pt – Sn (core)	ampptsn*		delrptsn*	ssptsn*
	Pt – Pt (shell)	amppth2		delrpth2	sspth2
	Pt – Sn (shell)	ampptsnh2		delrptsnh2*.*.*.*	ssptsnh2*.*.*.*
Sn K in H₂	Sn – O	ampsnoh2	enotpsnh2	delrsno**	sssno**
	Sn – Pt (core)	12×(1-ampsno) *		delrptsn*	ssptsn*
	Sn – Pt (shell)	ampsnpth2		delrptsnh2*.*.*.*	ssptsnh2*.*.*.*
	Sn – Sn (2 nd shell)	ampsnsnh2		delrsnsn**	sssnsn**

*Pt – Pt, Pt – Sn and Sn – Pt of the air data are set to have the same parameters as the core part of the H₂ data in terms of N , ΔR and σ^2 ;

** Sn – O and Sn – Sn (2nd shell) of the Sn edge data are set to have same ΔR and σ^2 ;

*** Pt – Sn and Sn – Pt of data measured in the same atmosphere are set to have same ΔR and σ^2 .

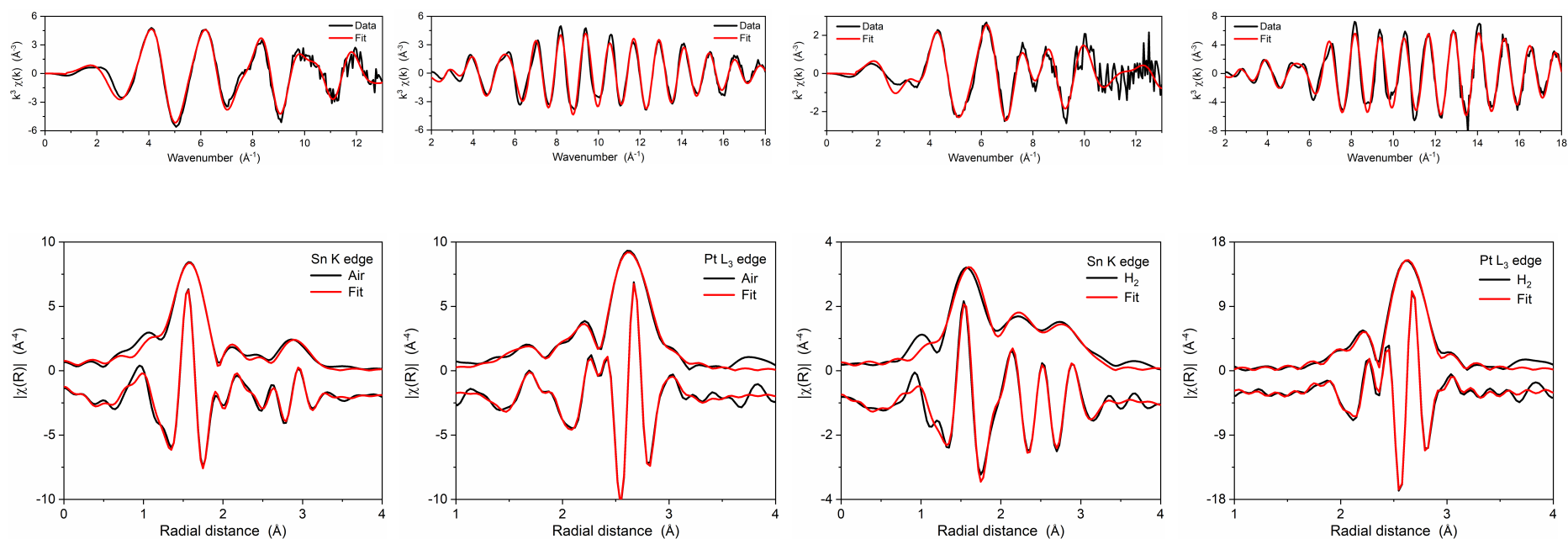


Figure S17 A 4-dataset fit for all EXAFS data of the dealloyed Pt-Sn, combining the data collected (1st and 2nd columns) in air and (3rd and 4th columns) in H₂, (1st and 3rd columns) at Sn K edge and (2nd and 4th columns) at Pt L₃ edge. The fit is shown in both (top) k^3 -weighted EXAFS spectra and (bottom) their Fourier transforms plotted as the magnitude and the real part (offset toward lower magnitude for clarity). The Fourier transformation was carried out in k -ranges of 3.6–12.4 Å⁻¹ for the Sn K-edge and of 3.5–18.0 Å⁻¹ for the Pt L₃ edge, and the fit was performed in R ranges of 1.2–3.2 Å for the Sn K-edge and of 1.2–3.0 Å for the Pt L₃ edge, using a fitting model with guess parameters listed in Table S4. The fit yields an R -factor of 0.38% and the obtained structural parameters listed in Table 2.

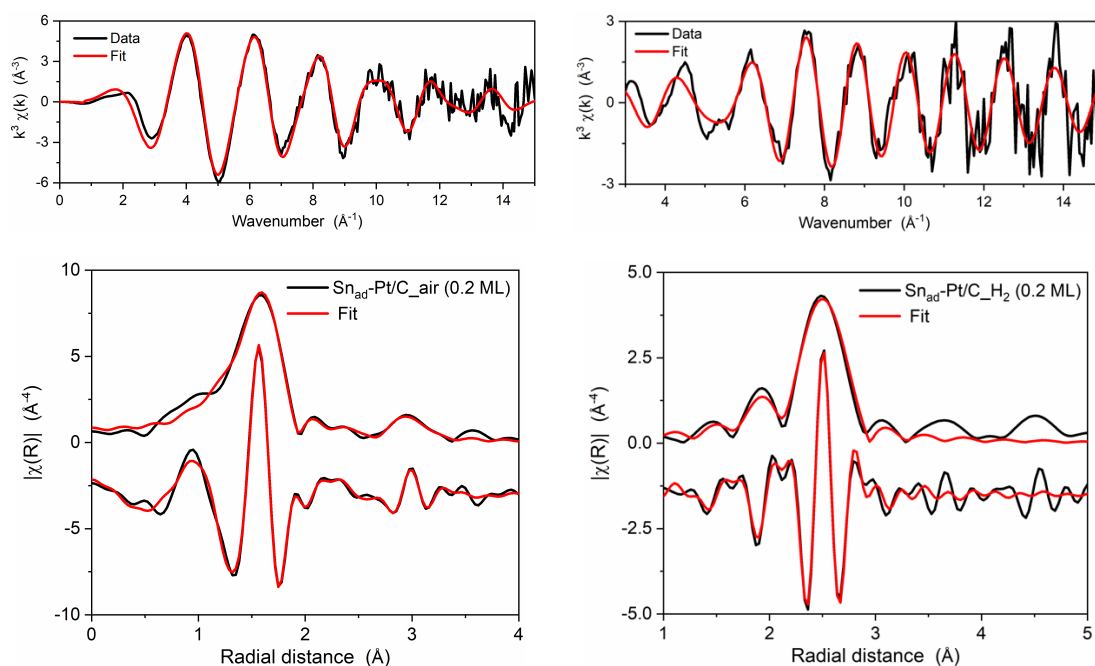


Figure S18 Fits for Sn K-edge EXAFS spectra of the Sn_{ad}-Pt/C sample (0.2 ML Sn coverage), showing as k^3 -weighted (top panels) k space and (bottom panels) the magnitude and the real part of R space. Both the spectra measured in (left panels) air and (right panels) H₂(g) are shown. For the air data, The Fourier transformation was performed in a k range of 3.4–14.0 Å⁻¹, and the fitting was carried in a R -range of 1.0–3.2 Å, and for the H₂ data, the Fourier transformation was performed in a k range of 5.8–14.0 Å⁻¹, and the fitting was carried in a R -range of 1.2–3.2 Å.

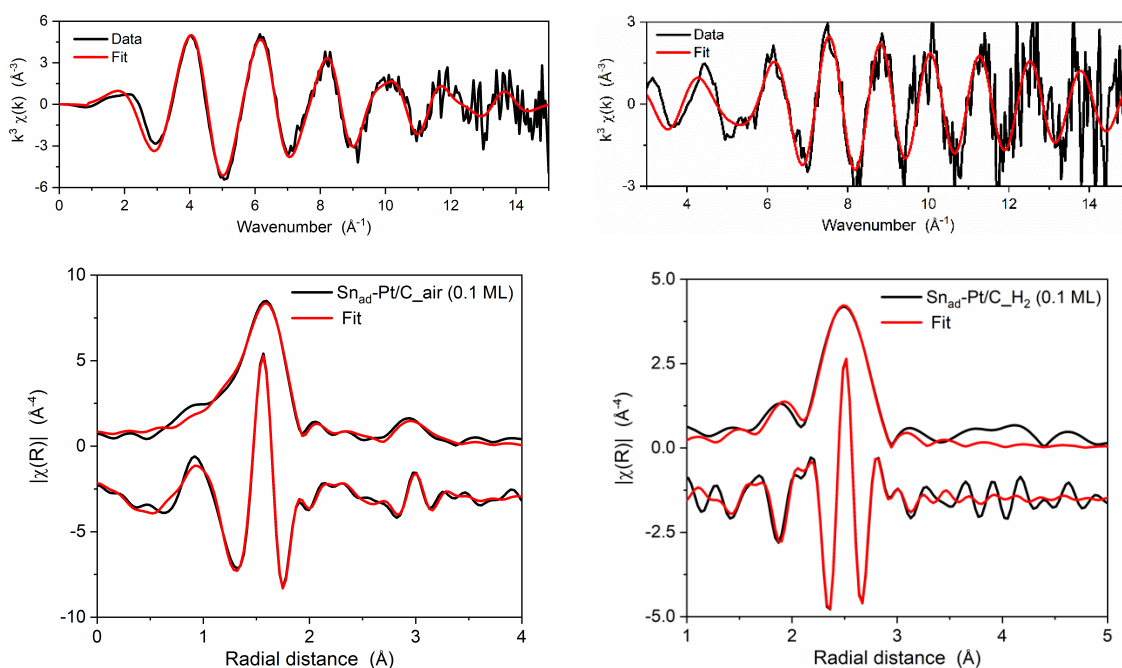


Figure S19 Same as Figure S18 but for a Sn_{ad}-Pt/C sample with a Sn coverage of 0.1 ML.

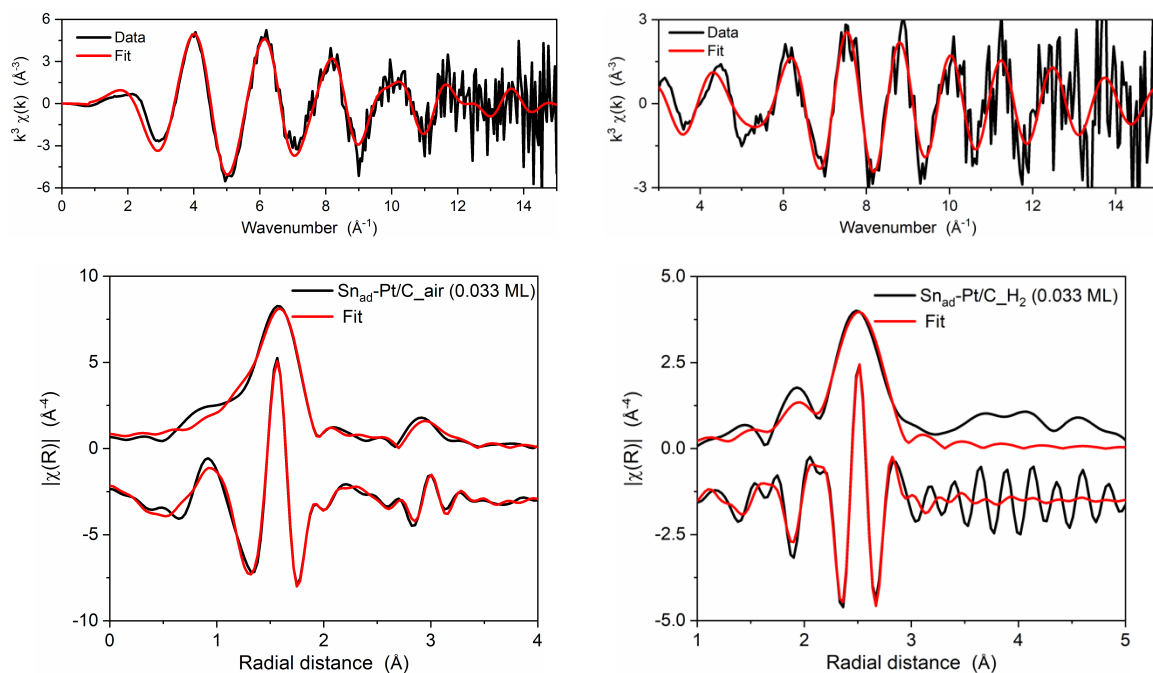


Figure S20 Same as Figure S18 but for a $\text{Sn}_{\text{ad}}\text{-Pt/C}$ sample with a Sn coverage of 0.033 ML.

Table S5 Structural parameters of $\text{Sn}_{\text{ad}}\text{-Pt/C}$ (Sn coverage from 0.2 ML to 0.033 ML), obtained from EXAFS fitting. Plots of the data and the corresponding fits are shown in Figure S18–Figure S20.

Sample	Scattering path	R (Å)	N	σ^2 ($\times 10^3 \text{ \AA}^2$)	ΔE_0 (eV)	R factor (%)
0.2 ML_Air	Sn – O	2.051(3)	6.4(2)	6.6(4)	2.2(4)	0.26
	Sn – Sn	3.272(9)	1.6(4)	9(2)		
0.1 ML_Air	Sn – O	2.051(6)	6.5(3)	7.1(8)	2.1(8)	1.1
	Sn – Sn	3.28(2)	1.3(7)	7(3)		
0.033 ML_Air^a	Sn – O	2.052(4)	6.3(2)	7.1(5)	2.6(6)	0.42
	Sn – Sn	3.28(1)	0.8(4)	6(3)		
0.2 ML_H₂^a	Sn – Pt	2.690(7)	4.5(4)	8.8(6)	-3(1)	1.17
0.1 ML_H₂	Sn – Pt	2.687(6)	4.8(4)	9.1(5)	-4(1)	0.86
0.033 ML_H₂^b	Sn – Pt	2.70(1)	5.7(9)	10(1)	-2(2)	2.71

^a Fluorescence data were used for increasing signal-to-noise level, and no obvious self-adsorption was found in these data.

Supplementary note 1: XANES and EXAFS analysis on SnO₂-Pt/C

SnO₂-Pt/C, synthesised by hydrolysing SnO₃²⁻ on a commercial Pt/C, is a controlled sample to ascertain the shortened Pt-Sn bond distance on the surface and to support the *R*-CN correlation in Pt-Sn system. The Sn speciation of the SnO₂-Pt/C samples was characterized by XANES (Figure S21) and EXAFS (Figure S22). The XANES spectrum of the SnO₂-Pt/C samples at Sn K edge was compared with that of the standard SnO₂. Like the dealloyed Pt-Sn, the SnO₂-Pt/C largely follows SnO₂ reference in terms of major features and the edge position, but slightly higher whiteness intensity is found, 1.53 for SnO₂-Pt/C and 1.50 for SnO₂. On the EXAFS spectra, compared to the previous Pt-Sn samples, the SnO₂-Pt/C shares the similar oscillations in phase with the SnO₂ in not only the first shell Sn-O region but also the higher shell Sn-Sn region, indicating that the ordered rutile SnO₂ structure is present. In terms of magnitude, these oscillations in these two regions are slightly weaker than those in SnO₂. The lower magnitude in the Sn-Sn region can be attributed to the smaller particle size of SnO₂ particles, but that in the Sn-O region could be from the lower CN, the lower extent of order, or both.

The corresponding EXAFS fitting (Figure S23 and Table S6) suggests that the CN of the Sn-O is 6.2±0.3, within the error with that of SnO₂, and the σ^2 ($6.0\pm 0.6\times 10^3 \text{ \AA}^2$), which describes the disorder degree of the Sn-O bond, is significantly higher than that of SnO₂ ($3.9\pm 0.5\times 10^3 \text{ \AA}^2$, Table 1) but close to the disordered [Sn^{IV}O₆] species on the Pt-Sn samples ($5\sim 6 \times 10^3 \text{ \AA}^2$). Thus, the lower magnitude in the Sn-O region is due to a fraction of disordered structure, and both disorder [Sn^{IV}O₆] species and order SnO₂ nanocrystals (from the presence of Sn-Sn scattering paths) coexist in the SnO₂-Pt/C.

Like the Pt-Sn samples, SnO₂-Pt/C can be partly reduced by H₂ at room temperature, as indicated by changes in whiteness intensity and edge position. However, for the edge position, the change is not a simple shift but a broadened shoulder toward lower energy, which indicates that the extent of reduction is limited, and a significant amount of tin oxide remains after H₂ reduction. The same indication can also be found in the EXAFS. The CN of the Sn-O decreased less than half to 3.4±0.2, lower than that of the dealloyed Pt-Sn sample. In addition, in the Sn-Sn regions the oscillations are largely unchanged in terms of phase and magnitude. Thus, for the reduction of Sn^{IV} species in the SnO₂-Pt/C, only part of the [Sn^{IV}O₆] species was participated and reduced into Sn-Pt bonds, and the crystallized SnO₂ was not

involved. The distinct reactivity between the disordered [Sn^{IV}O₆] and crystalized SnO₂ is consistent with a study of tin oxide on Pt(111) by ambient pressure X-ray photoelectron spectroscopy study². In this study, the disordered tin oxide is found to be highly active and can be reduced by H₂ at low partial pressure of H₂ and low temperature, whilst other tin oxide film, ordered monolayers and multilayers, were found to show much lower reduction activity by 7 orders of magnitude.

For the EXAFS fit of the H₂ data, three scattering paths, one Sn–Pt and two Sn–Sn, are involved in a narrow *R* range of 2.5~3.5 Å, and 13 variables are required out of ~18 independent points fits (Figure S23 and Table S6). To have sufficient independent points and to obtain more precise structural parameters, a constrained fit was proposed. In this fitting model, the *R* and σ^2 of the inactive tin oxide phases are assumed to be unaffected by the H₂ reduction, which can be inferred from the individual. The double-data-set fit produces approximate structural parameters of the air data as compared to the individual fit and yields a more reasonable parameter (Figure S24 and Table S7).

More importantly, a shortened and precise Sn-Pt bond (2.768±0.007 Å) is obtained. Assuming the residual tin oxide species in H₂ have a saturated O shell in H₂, the CN of the surface Sn atoms can be estimated to be 8.8±1.7. Same EXAFS analysis was also applied to a SnO₂-Pt/C sample from a different branch (SnO₂-Pt/C_2), and the CN of the shortened Sn-Pt (*R*=2.771±0.009 Å) is 9.2±2.4 (Figure S25 and Figure S26, Table S8 and Table S9).

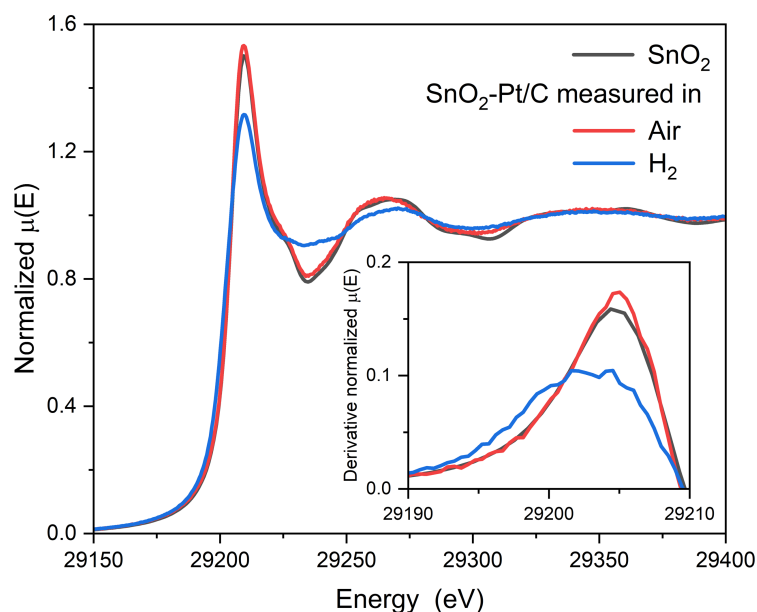


Figure S21 Sn K-edge XANES spectra of SnO₂-Pt/C samples collected in air and in H₂, along with (inset) the 1st derivative at the rising edge region. This figure shows the reduction of Sn species as suggested by the decreased intensity of whiteline and the negative shift of the rising edge.

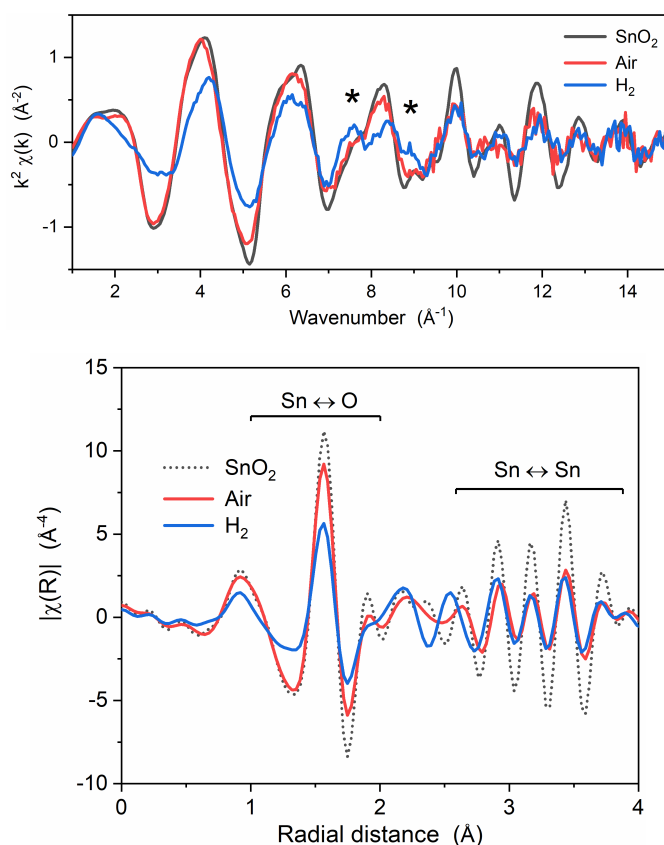


Figure S22 Sn K-edge EXAFS spectra of SnO₂-Pt/C samples in (top) k space and (bottom) the real part of R space. The samples collected in air and collected in H₂ are present, and the spectra are k^2 -weighted. The comparison of the samples indicates the H₂ reduction induces a decreased intensity in

low k -region (3–6 \AA^{-1}) and low R -region (1–2 \AA) and an added oscillation at 7–9 \AA^{-1} and 2–3 \AA . This indicates the Sn coordination is altered due to the H_2 reduction.

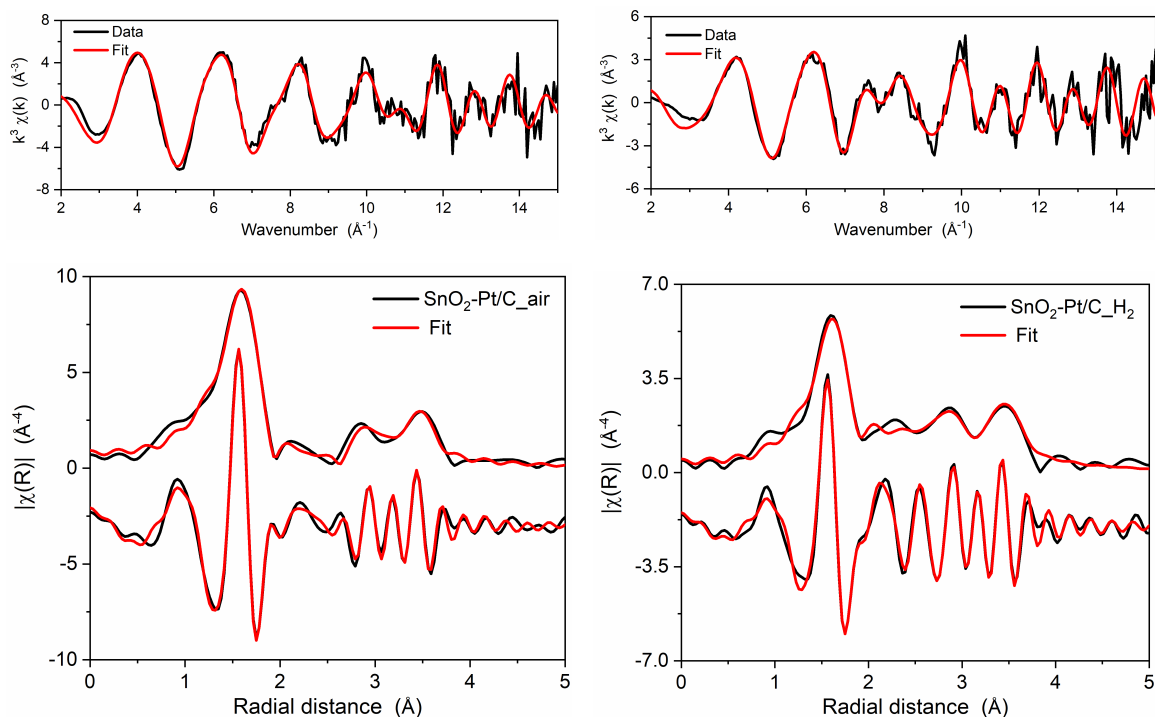


Figure S23 Individual fits for Sn K-edge EXAFS spectra of SnO_2 -Pt/C samples (measure in air and in H_2), plotted as k^3 -weighted (top panels) k -space and (bottom panels) the magnitude and the real part of R -space. The Fourier transformation was performed in a k -range of 3.4–14.0 \AA^{-1} , and the fitting was carried in an R -range of 1.0–3.7 \AA , yielding R-factors of 0.57% for the air data and 0.76% for the H_2 data. The obtained structural parameters are listed in Table S6.

Table S6 Structural parameters obtained from the individual fits of SnO_2 -Pt/C data. The fits use 10 variables out of ~ 18 independent points for the air data and 13 out of ~ 18 for the H_2 data.

Sample	Scattering path*	R (\AA)	N	σ^2 ($\times 10^3 \text{\AA}^2$)	ΔE_0 (eV)	R factor (%)
SnO_2-Pt/C (air)	Sn–O	2.052(5)	6.2(3)	6.0(6)		
	Sn–Sn (2 nd shell)	3.23(1)	0.9(4)	5(2)	3.1(6)	0.57
	Sn–Sn (3 rd shell)	3.721(9)	0.9(5)	2(2)		
SnO_2-Pt/C (H_2)	Sn–O	2.054(9)	3.4(2)	6(1)		
	Sn–Pt	2.77(1)	4(1)	11(2)	5(1)	0.76
	Sn–Sn(2 nd shell)	3.22(3)	0.3(4)	4(6)		

Sn–Sn(3 rd shell)	3.72(1)	0.6(4)	1(3)
------------------------------	---------	--------	------

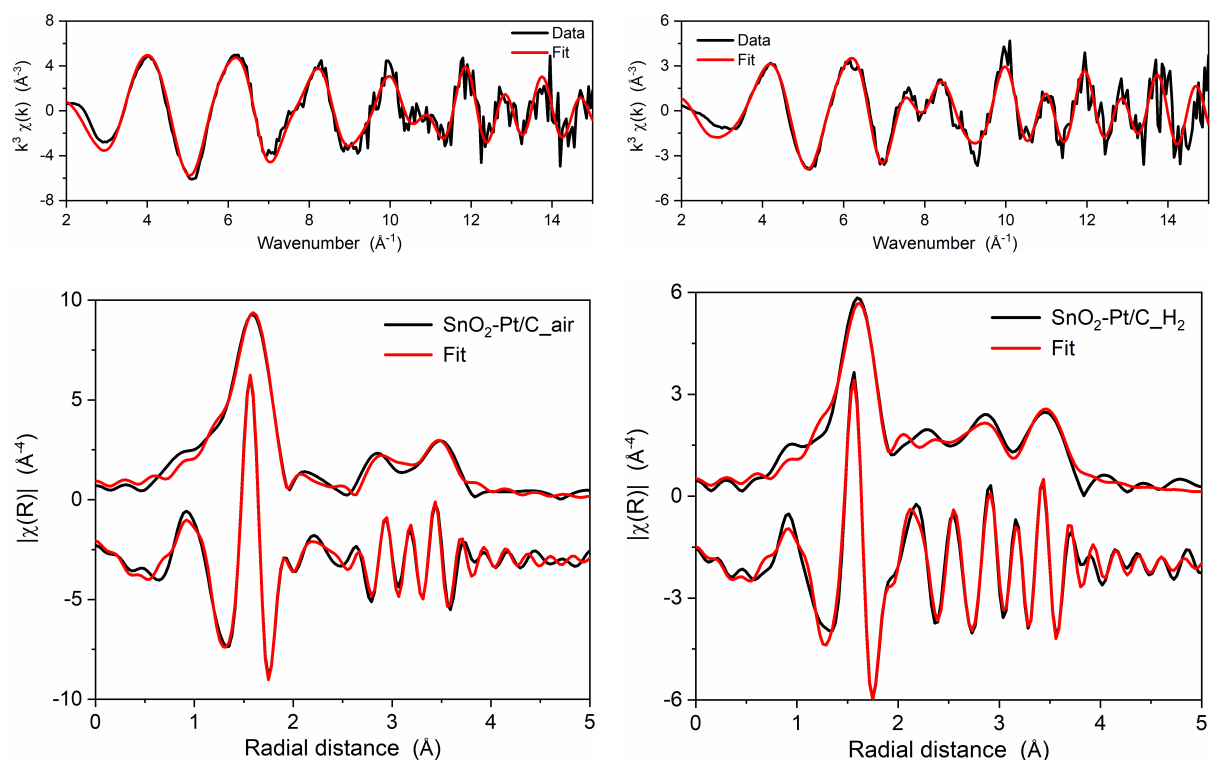


Figure S24 A double-dataset fit for Sn K-edge EXAFS spectra of SnO₂-Pt/C samples, combining the data measured in air and that in H₂. The fit is plotted as k^3 -weighted (top panels) k -space and (bottom panels) the magnitude and the real part of R -space. The Fourier transformation was performed in a k -range of 3.4–14.0 Å⁻¹, and the fitting was carried in an R -range of 1.0–3.7 Å, yielding an R-factor of 0.74% and the obtained structural parameters listed in Table S7.

Table S7 Structural parameters obtained from the combined dataset fit of SnO₂-Pt/C samples. The fit uses 17 variables out of ~36 independent points.

Sample	Scattering path	R (Å)	N	σ^2 ($\times 10^3$ Å ²)	ΔE_0 (eV)	R factor (%)
SnO ₂ -Pt/C (air)	Sn–O*	2.053(4)	6.2(2)	5.9(4)		0.74
	Sn–Sn (2 nd shell)*	3.23(1)	0.9(3)	5(2)	3.1(5)	
	Sn–Sn (3 rd shell)*	3.719(5)	0.8(3)	1(1)		
SnO ₂ -Pt/C (H ₂)	Sn–O*	2.053(4)	3.4(1)	5.9(4)		0.74
	Sn–Pt	2.768(7)	3.8(7)	11(1)	5.1(6)	
	Sn–Sn (2 nd shell)*	3.23(1)	0.4(2)	5(2)		

Sn-Sn (3rd shell)* 3.719(5) 0.7(2) 1(1)

* For SnO₂-related scattering paths, Sn-O, Sn-Sn₁(2nd shell) and Sn-Sn₁(3rd shell), each path is set to have the same R and σ^2 for both the air data and the H₂ data. Highlighted in blue.

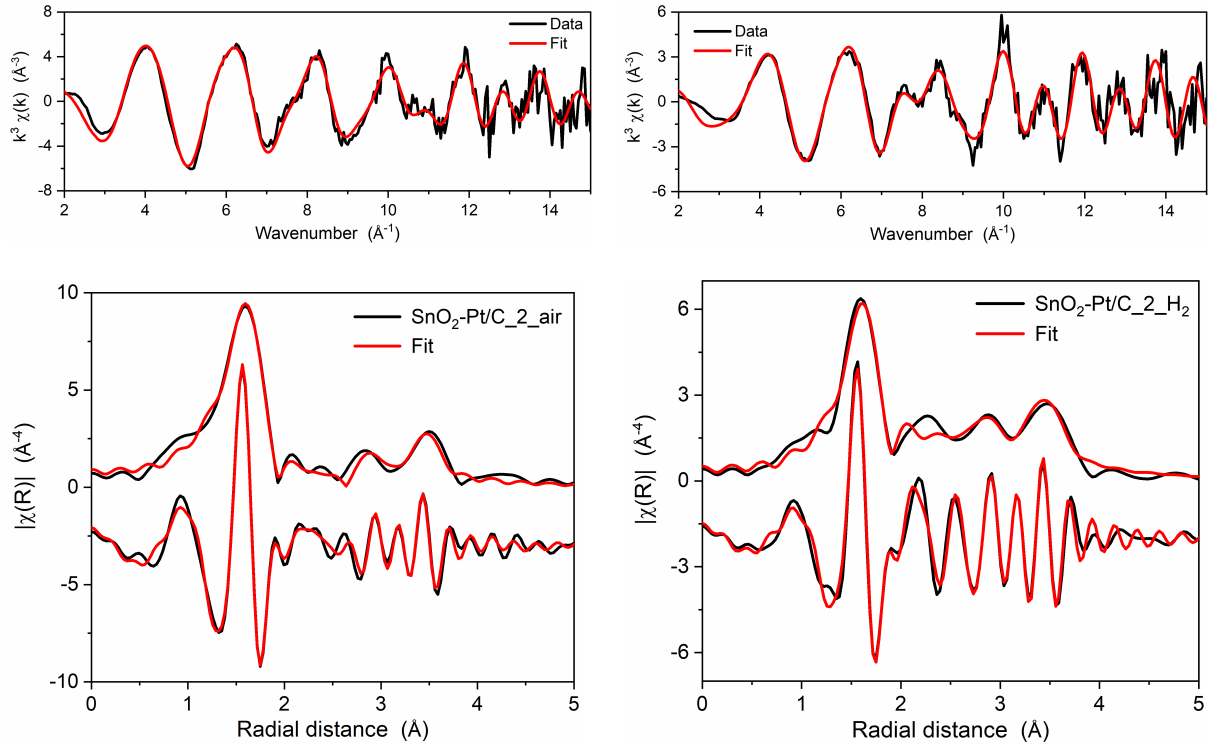


Figure S25 Same as Figure S23 but for SnO₂-Pt/C_2. The obtained parameters are listed in Table S8.

Table S8 Structural parameters obtained from the individual fits of SnO₂-Pt/C_2 data. The fits use 10 variables out of ~18 independent points for the air data and 13 out of ~18 for the H₂ data.

Sample	Scattering path*	R (Å)	N	σ^2 ($\times 10^3$ Å ²)	ΔE_0 (eV)	R factor (%)
SnO₂-Pt/C_2 (air)	Sn-O	2.051(5)	6.2(3)	5.8(6)		
	Sn-Sn (2 nd shell)	3.24(1)	1.1(5)	7(3)	3.2(6)	0.67
	Sn-Sn (3 rd shell)	3.72(1)	1.0(5)	2(2)		
SnO₂-Pt/C_2 (H₂)	Sn-O	2.046(9)	3.2(3)	5(1)		
	Sn-Pt	2.77(1)	5(2)	13(3)	5(2)	1.3
	Sn-Sn(2 nd shell)	3.20(5)	0.4(6)	5(8)		

Sn–Sn(3 rd shell)	3.72(1)	0.6(5)	0.3(30)
------------------------------	---------	--------	---------

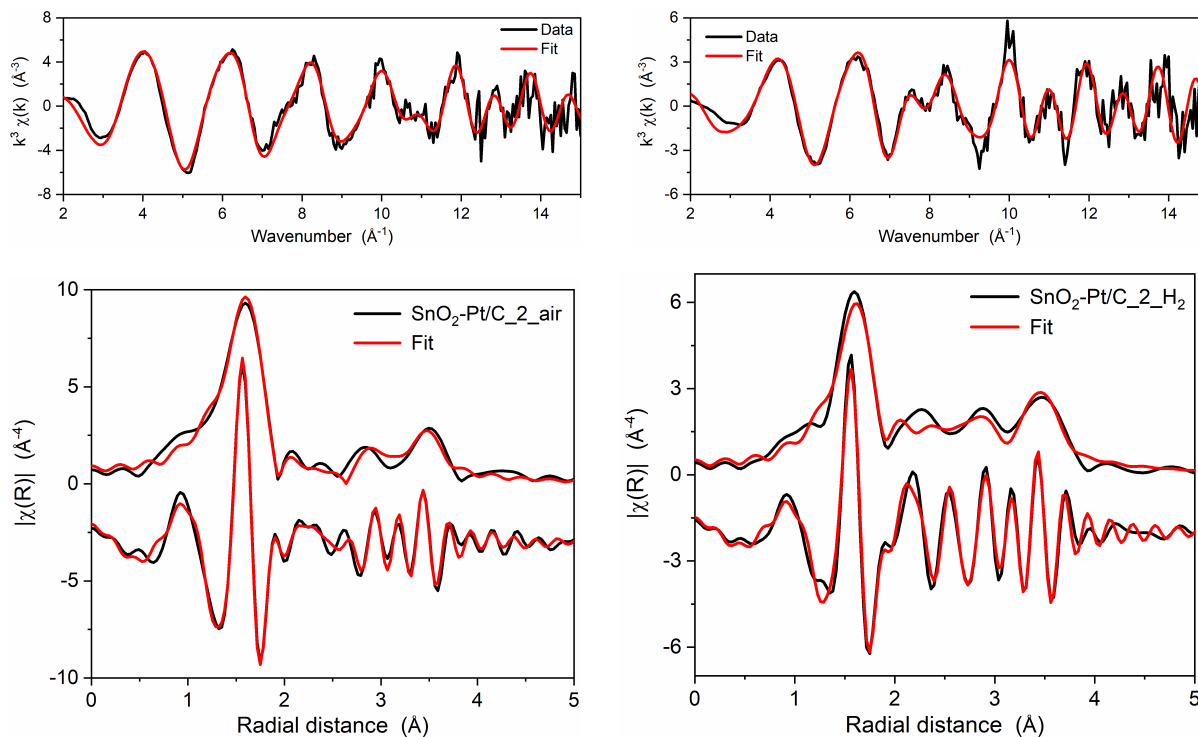


Figure S26 Same as Figure S24 but for SnO₂-Pt/C₂. The obtained parameters are listed in Table S9.

Table S9 Structural parameters obtained from the combined dataset fit of SnO₂-Pt/C samples. The fit uses 17 variables out of ~36 independent points.

Sample	Scattering path	R (Å)	N	σ^2 ($\times 10^3$ Å ²)	ΔE_0 (eV)	R factor (%)
SnO₂-Pt/C₂ (air)	Sn–O*	2.050(4)	6.1(2)	5.5(5)		1.2
	Sn–Sn (2 nd shell)*	3.23(1)	1.0(4)	6(3)	3.1(6)	
	Sn–Sn (3 rd shell)*	3.719(6)	0.7(3)	1(2)		
SnO₂-Pt/C₂ (H₂)	Sn–O*	2.050(4)	3.4(2)	5.5(5)		1.2
	Sn–Pt	2.771(9)	4(1)	12(2)	5.0(7)	
	Sn–Sn (2 nd shell)*	3.23(1)	0.5(3)	6(3)		

Sn-Sn (3rd shell)* 3.719(6) 0.8(3) 1(2)

* For SnO₂-related scattering paths, Sn-O, Sn-Sn₁(2nd shell) and Sn-Sn₁(3rd shell), each path is set to have the same R and σ^2 for both the air data and the H₂ data. Highlighted in blue.

References

1. H. Huang, A. Nassr, V. Celorrio, S. F. R. Taylor, V. K. Puthiyapura, C. Hardacre, D. J. L. Brett and A. E. Russell, *Faraday Discuss.*, 2018, **208**, 555-573.
2. L. Y. Kraya, G. F. Liu, X. He and B. E. Koel, *Top. Catal.*, 2016, **59**, 497-505.